Available online at www.sciencedirect.com
SCIENCE DIRECT
Journal of Catalysis 232 (2005) 10–18
JOURNAL OF CATALYSIS
www.elsevier.com/locate/jcat

Transformation of platinum supported on silicon-doped alumina during the catalytic decomposition of energetic ionic liquid

L. Courtheoux, E. Gautron, S. Rossignol *, C. Kappenstein

University of Poitiers, LACCO UMR 6503, Laboratoire de Catalyse par les Métaux, 40 Avenue du Recteur Pineau, F-86022 Poitiers cedex, France

Received 8 November 2004; revised 2 February 2005; accepted 3 February 2005

Available online 7 April 2005

Abstract

The stability of 10 wt% platinum supported on Si-doped alumina (Pt/Si–Al_2O_3) during the catalytic decomposition of energetic ionic liquid (or propellant) at 40 °C was studied. The reaction was performed by successive injections of 79 wt% HAN (hydroxylammonium nitrate NH_3OHNO_3) aqueous solution onto the catalysts in a constant volume batch reactor. The four studied catalysts remain active with a fast reaction rate (up to 450 mbar s^{-1}), even in the presence of an excess of residual aqueous solution. For all catalysts, the structural studies reveal the presence of theta alumina associated with silica and platinum particles. After the propellant decomposition, alteration in metallic particle size is observed as is the formation of nanosized platinum agglomerates in the reaction medium, which are probably responsible for the excellent catalytic activity. A model is suggested, explaining the part played by platinum and silica particles at the surface of the materials during the propellant decomposition reaction.

Keywords: Sol–gel; Platinum-based catalysts; Ionic liquid; Doped alumina; Characterizations; XRD; TEM

1. Introduction

Energetic liquid compounds known as monopropellants are used for propulsion and gas generation. For example, the orbit and attitude control of satellites is achieved with small thruster engines, with the use of the catalytic decomposition of liquid hydrazine (N_2H_4) on supported iridium catalysts (Ir/Al_2O_3) [1]. The high toxicity of this monopropellant creates high storage and handling costs due to more severe regulation rules, and its replacement by less toxic propellants is of current interest [2–5]. The most currently proposed and studied hydrazine substitutes are energetic ionic liquids and a representative mixture containing hydroxylammonium nitrate (HAN, $NH_3OH^+NO_3^-$) as an oxidizer, water, and an ionic or molecular fuel as a reducer [6–10]. However, such mixtures involve more drastic conditions because of the high temperature reached during the decomposition (adiabatic temperature up to 1800 °C) and the need for frequent restarts that involve preheating of the catalyst (300–400 °C), which is currently a drawback for the development of the engine. Therefore, a high catalytic activity at lower temperature (20–200 °C) associated with a high thermal stability of the catalysts is a critical parameter for the future development of new engines.

Previous studies performed by our group have shown that platinum supported on thermally stable silicon-doped alumina displays a good activity at low temperatures [11]. The Si-doped alumina support is obtained by the sol–gel procedure, and the introduction of the silicon precursor makes possible better thermal stabilization of the transition alumina [12]. The catalysts are then evaluated for the decomposition of propellants with the use of a lab-made constant volume batch reactor [7]. The decomposition of a HAN–water mixture on these catalysts begins at a very low temperature, 40 °C or less [13], whereas the thermal decomposition temperature is in the range of 115–120 °C [9]. Another key point concerns the long-term stability of the catalysts, particularly in the presence of a large amount of propellant. Most of the

* Corresponding author. Fax: 33 (0)5 49 45 40 20.
E-mail address: sylvie.rossignol@univ-poitiers.fr (S. Rossignol).

0021-9517/$ – see front matter
doi:10.1016/j.jcat.2005.02.005

papers concerning this topic are available as AIAA conference proceedings [14].

The objectives of this work were to evaluate the catalytic activity during several successive injections of propellant, in order to simulate the pulse mode of the satellite thrusters, and to characterize the catalysts before and after the reaction, by X-ray diffraction (XRD), transmission electron microscopy (MET), and specific surface area measurements (S_{BET}).

2. Experimental

All catalysts are based on 10 wt% platinum supported on silicon-doped alumina. The support was prepared in our laboratory by the sol–gel method and has already been described [15,16]. We have prepared samples of nominal composition $(Al_2O_3)_{0.88}$–$(SiO_2)_{0.12}$ (atomic Si/Al ratio 6:94) according to the Yoldas procedure [17] under an excess of water (H_2O/Al molar ratio 100:1). The synthesis was performed with $Al(O–^{sec}C_4H_9)_3$ as a molecular precursor. After 1 h at 60 °C, the corresponding amount of $Si(OC_2H_5)_4$ was slowly added, followed by a small quantity of HCl (Al + Si/HCl molar ratio 1:0.07). The temperature was raised to 80 °C and maintained for 2 h in a covered beaker to avoid solvent evaporation. Then the beaker was left open for several hours at the same temperature, and gelling occurred. After gelling and cooling, the sample was dried at 120 °C for 12 h in an oven, leading to the xerogel form, and was then fired for 5 h at 1200 °C.

The metallic phase (10 wt%) is introduced by impregnation of H_2PtCl_6 precursor solution, followed by reduction (r) at 400 °C (4 h). The sample name is 10rx (10 for 10 wt% Pt; r for reduced sample; x for xerogel support). Some catalysts have been prepared from two successive impregnations, each corresponding to 5 wt% platinum, on xerogel supports, with an intermediate reduction between impregnations (sample 5r + 5rx) or without this intermediate reduction (sample (5 + 5r)x). For development applications, a sphere-shaped sample (1 mm diameter) was made from a xerogel powder and impregnated with the platinum precursor (three impregnations followed by reduction for a total of 10 wt% Pt); this sample is called 3i.Pt.MF.

The specific surface area of the samples was determined by the BET method from the nitrogen adsorption isotherms at −196 °C in an automated Micromeritics Tristar 3000 apparatus after drying for 90 min at 350 °C. Particle sizes were determined by X-ray diffraction experiments performed on a Siemens D 5005 powder θ–θ diffractometer with Cu-K_α radiation ($\lambda K_\alpha = 0.15418$ nm) and a secondary graphite back monochromator. The diffractograms were obtained under the following conditions: dwell time: 2 s; step: 0.04° 2θ; divergence slit: 1°. The crystalline phases were identified by comparison with ICDD standards (PDF number: θ alumina: 23-1009; platinum: 04-0802). The crystallite sizes were determined with the Scherrer equation [18]. A transmission electron microscope (Philips CM 120) coupled with an energy dispersive X-ray spectrometer (EDX) made it possible to determine the particle size and the distribution of Pt, Al, and Si atoms by X-ray mapping at the corresponding energies (Pt-L_α at 9.441 keV; Al-K_α at 1.486 keV; Si-K_α at 1.739 keV).

We performed the catalyst evaluation by decomposing an aqueous solution of HAN (79 wt% hydroxylammonium nitrate; $NH_3OH^+NO_3^-$) in a constant volume batch reactor (167 cm^3) [7], in the increase temperature mode or the isothermal mode at 40 °C. This last temperature was specified in a previous work, where we could show that the prepared 10 wt% Pt catalysts permitted the decomposition of the HAN solution at about 40 °C [13]. When the catalyst is heated from the bottom, the reactor displays a temperature gradient, in which the top is the cold part; thus the gas temperature is lower than the catalyst temperature. In the temperature increase mode, 100 µl of propellant (1.23 mmol; density 1.50 g cm^3) is injected at room temperature on 160 mg of catalyst, and the reactor is heated with a ramp of 10 K min^{-1}. For the isothermal mode, we proceeded to make successive manual injections of 100 µl of propellant (i.e., 150 mg, 1.23 mmol HAN) on 160 mg of catalyst. Each injection led to fast increases in pressure and temperature, which returned to equilibrium values within 3 to 4 min; therefore, each injection was carried out after an interval of approximately 4 min. Pressure and temperature variations against time made it possible to determine the evolution of the catalyst performances in the presence of a large cumulative amount of propellant (HAN/Pt molar ratio in the range of 225–323 for 15 injections).

To identify the gaseous reaction products, a dynamic reactor was designed [19]. This was a fixed-bed reactor with online analysis by a mass spectrometer (Omnistar; Pfeiffer, Quadstarr 422 software). The catalyst (160 mg) was put into a quartz reactor and was preheated at 40 °C. Fifteen successive injections of HAN solution were performed every 4 min.

3. Results

3.1. Catalytic tests: temperature increase mode

The experiments in temperature increase mode allowed us to determine the onset decomposition temperature of the monopropellant for the different catalysts, the pressure increase due to the formation of gaseous products, and a "reaction rate" defined as the slope of the pressure increase, as shown in Fig. 1. We observed a pressure spike followed by a step and a temperature peak reaching 120 °C; the temperature decrease was due to the thermal transfer to the reactor. The results are presented in Table 1; all prepared catalysts are very promising because they display very low decomposition temperatures: 62 °C for the sphere-shaped catalyst and 22–33 °C for the powdered catalysts. The pressure increases are on the same order of magnitude (about 120 mbar), and

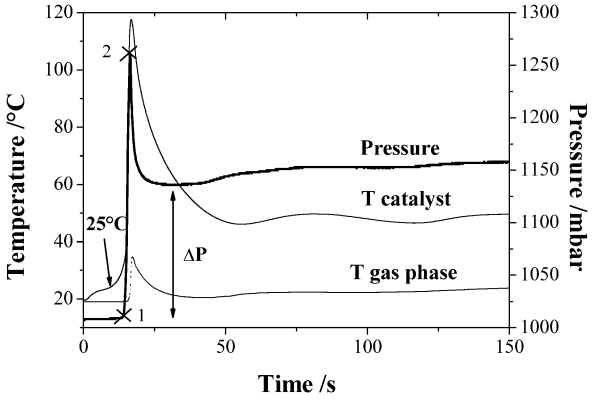

Fig. 1. Pressure and temperature (gaseous phase and catalyst) versus time during the decomposition of 79 wt% HAN (100 µl) in the temperature increase mode (10 K min^{-1}) on the (5 + 5)rx catalyst (160 mg), pressure increase (ΔP) and slope between points 1 and 2.

Table 1
79 wt% HAN onset decomposition temperature, pressure increase and slope for the reaction in temperature increase mode for various catalysts

Name	T (°C)	ΔP (mbar)	Slope (mbar s^{-1})
10rx	22	126	87
5r + 5rx	33	119	73
(5 + 5)rx	25	129	120
3i.Pt.MF	62	123	107

the best reaction rate is observed for the (5 + 5)rx catalyst (120 mbar s^{-1}), measured by at least 5 points. For the catalyst 3i.Pt.MF, we observed, after the reaction, a mechanical breaking of the spheres, probably due to the strong exothermicity and pressure increase in the pores during the HAN decomposition. This mechanical breaking could be avoided by preheating at higher temperature, as is the case for hydrazine decomposition [1]; this preheating helps to accelerate the decomposition and thus to avoid accumulation of liquid inside the pore. Thus the local overpressure and the mechanical strains inside the pores during the decomposition were limited.

3.2. Catalytic tests: constant-temperature mode

A typical example of temperature and pressure evolution versus time during 15 successive injections is shown in Fig. 2(a) for the 10rx catalyst preheated at 40 °C. The samples display a significant activity after 15 propellant injections. After each injection, we observe a pressure spike due to the high decomposition rate, followed by a step. The gas phase and catalyst temperatures display peaks due to the exothermic decomposition reaction followed by heat transfer to the reactor wall and retrieval of the initial temperature (25 °C for the gas phase and 40 °C for the catalyst). During HAN decomposition, the amount of water present in the sample holder increases, because only a fraction is vaporized and condenses at the top of the reactor (cold part). Therefore, the maximum temperature reached by the catalyst is

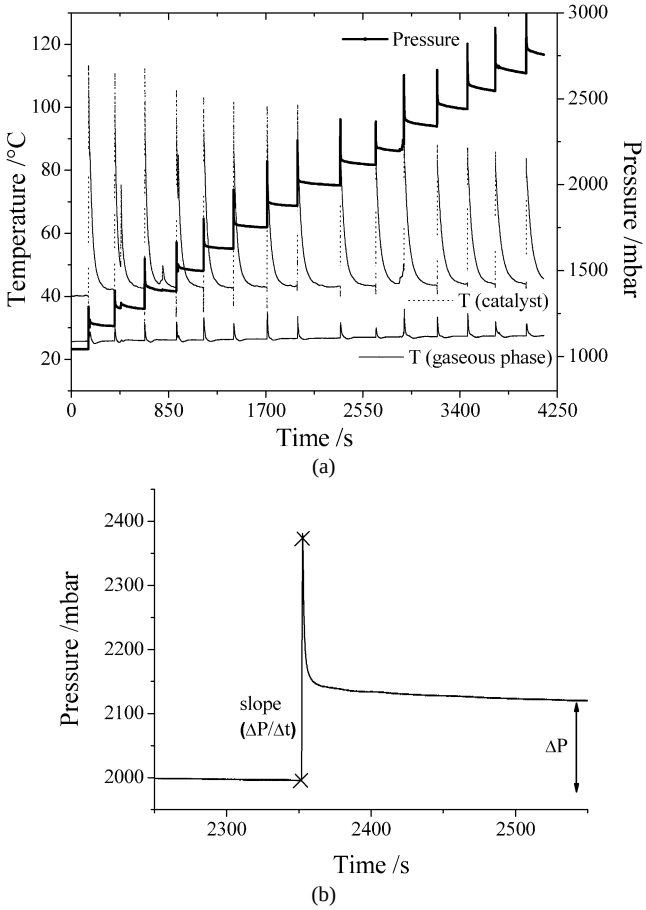

Fig. 2. (a) Pressure and temperature (gaseous phase and catalyst) versus time during 15 injections of 79 wt% HAN solution at 40 °C on the 10rx catalyst (160 mg; 15 × 100 µl); (b) enlargement to determine pressure increase and slope.

gradually decreasing (112 to 80 °C) because of the increasing amount of water (as reactant in the HAN solution and product) in the sample holder, up to about 1.1 cm^3 after 15 injections. Another important feature is the ability of the catalyst to maintain a good activity in the presence of this water excess.

HAN decomposition can lead to thermodynamic products (water, nitrogen, and oxygen, Eq. (1)) or kinetic products (nitrogen oxides, Eqs. (2), (3), and (4)) [20–22]. The reaction enthalpy, taking into account the composition of the solution, is given in parentheses ($\Delta_r H^\circ$ in kJ mol^{-1}) [23]

$$NH_3OHNO_{3(aq)} \rightarrow 2H_2O_{(l)} + N_{2(g)} + O_{2(g)} \quad (-227.7), \quad (1)$$

$$NH_3OHNO_{3(aq)} \rightarrow 2H_2O_{(l)} + 0.5N_{2(g)} + NO_{2(g\ or\ aq)} \quad (-193.5), \quad (2)$$

$$NH_3OHNO_{3(aq)} \rightarrow 2H_2O_{(l)} + 2NO_{(g)} \quad (-45.11), \quad (3)$$

$$NH_3OHNO_{3(aq)} \rightarrow 2H_2O_{(l)} + N_2O_{(g)} + 0.5O_{2(g)} \quad (-146.1). \quad (4)$$

Nitric acid was proposed as an intermediate reaction species [21], but we did not observe its quantitative forma-

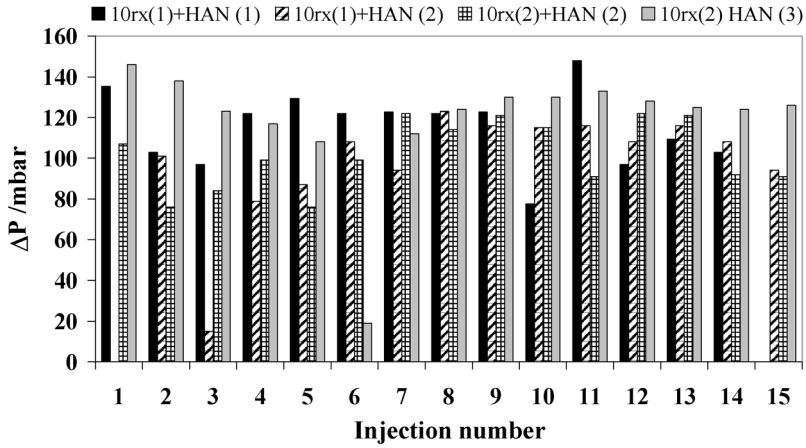

Fig. 3. ΔP values as a function of injection number for four experiments with different 79 wt% HAN–water and 10rx catalyst preparations at 40 °C.

Table 2
BET surface area, platinum content determined by CNRS analyses and particle size (from X-ray diffraction) before and after reaction at 40 °C for different samples. The last column gives the average of the ΔP value for the 15 injections

Catalysts	Before reaction			After 15 injections of HAN			ΔP average (mbar)	σ (ΔP) (mbar)
	BET ($m^2\ g^{-1}$)	% Pt (wt)	Size (Å)	BET ($m^2\ g^{-1}$)	% Pt (wt)	Size (Å)		
10rx	70	8.3	220	58	4.9	320	115	18
5r + 5rx	58	8.4	180	99	5.0	160	121	17
(5 + 5)rx	61	7.2	90	71	4.6	80	107	16
3i.Pt.MF	43	10.0	160	44	10.0	–	127	20

tion in the final products, the pH of residual water being between 2 and 3, due probably to the dissolution of nitrogen dioxide (vide infra).

The pressure increase (ΔP) and the pressure slope ($\Delta P/\Delta t$) were obtained for each peak from peak enlargement (Fig. 2b). To check the reproducibility of the results, the 15-injection test was performed four times with three independent HAN solution preparations and two 10rx catalyst preparations. The ΔP values for the successive injections are reported in Fig. 3 for four propellant–catalyst associations. The dispersion of the results is linked to the manual injection procedure, in which the syringe is filled and introduce through the septum for each injection. An automatic injection apparatus was built, from a remote-controlled microburette, but failed for this pulse injection mode. The pressure average and the corresponding standard deviation (given in parentheses; the two very low values were ignored) for each test were

Test 10rx(1) + HAN(1): 115(18) mbar;

Test 10rx(1) + HAN(2): 105(13) mbar;

Test 10rx(2) + HAN(2): 102(17) mbar;

Test 10rx(2) + HAN(3): 126(10) mbar.

The results display similar pressure increases, thus indicating both reproducibility and repeatability of the tests. Table 2 shows similar pressure averages for the different catalysts. The calculated pressure increase is in the range of 90 mbar (Eq. (2)) to 360 mbar (Eq. (1)). The experimental data are in between, in agreement with the formation of thermodynamic and kinetic products (vide infra, Fig. 5) and thus lead to the same selectivity [13].

In Fig. 4, we present the pressure slope as a function of the injection number. The results are very sensitive to the injection procedure, displaying a high dispersion that can take the form of some kind of oscillations. Nevertheless, we can deduce general trends: the average slope increases up to the seventh to ninth injection, then reaches a plateau. The very low-slope data corresponding to injection 11 (sample 3i.Pt.MF) or injections 14 and 15 (sample (5 + 5)rx) could be explained by a propellant drop reaching the side of the sample holder before coming into contact with the catalyst (which cannot be detected, as our reactor has no window). From these data, the catalysts can be ordered according to the following sequence:

$$(5 + 5)\text{rx} \sim \text{3i.Pt.MF} < 10\text{rx} < 5\text{r} + 5\text{rx}.$$

To identify the gaseous products formed during the monopropellant decomposition, catalytic tests were performed in the dynamic reactor, with the same injection procedure. The preliminary results deduced from these experiments (Fig. 5) reveal the very fast formation of N_2, NO, and O_2 as primary products. Then the formation of N_2O and traces of NO_2 are noted with parallel profiles. As for the thermal decomposition [13], the catalytic decomposition leads to the formation of kinetic and ther-

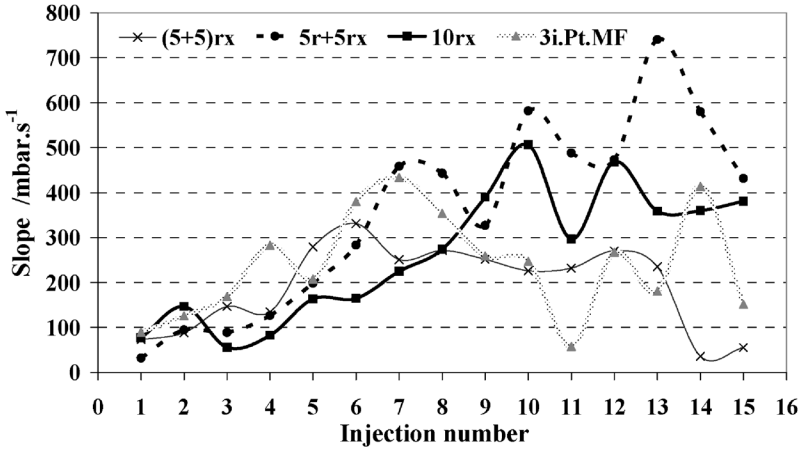

Fig. 4. Evolution of the slope ($\Delta P/\Delta T$) as a function of the injection number for different catalysts during 15 injections.

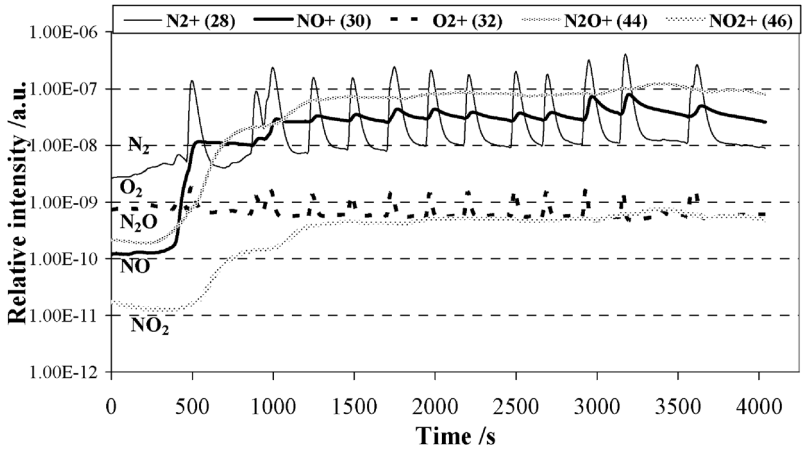

Fig. 5. Variation of the relative intensity of the main products as a function of time during 15 injections of $HAN_{79\%}$–water in the dynamic reactor at 40 °C on the 10rx catalyst.

modynamic products [19]. The different profiles for nitrogen oxides, by comparison with nitrogen and oxygen, can be related to slow adsorption–desorption equilibriums. Therefore, the experiments performed in two different reactors lead to similar results; to quantify these data, calibrations of the mass spectrometer are currently in progress, with the use of representative mixtures in the same conditions.

To supplement these results, different characterizations have been carried out, before and after the test reaction.

3.3. Structural data and morphology: before reaction test

The platinum loading content of the powdered samples (7–8.5 wt% Pt, Table 2) is always lower than the expected value (10 wt%), mainly because of weak platinum–carrier surface interactions; therefore part of the platinum is lost from the carrier surface during the thermal treatments. In contrast, for the sphere-shaped sample, this part remains inside the porosity, leading to the expected value.

BET surface area values measured before reaction (Table 2) are in accordance with the value determined for the corresponding support fired at 1200 °C (65 $m^2\,g^{-1}$) [6] despite the important platinum load.

XRD data (Fig. 6; 10rx catalyst as typical example) confirm the presence of θ-alumina in the support without change after impregnation and the platinum metal phase. The determination of crystallite size is based on the last two diffraction peaks (see enlargement in Fig. 6), where the contribution of the support is very weak. The high platinum contents (between 7 and 10%) induce a sufficient intensity of platinum diffraction peaks to determine the crystallite size. The comparison of our results with the literature data is not suitable because of the low amount of platinum generally used (0.1–2%) [24,25]. Three samples display almost the same average size in the range 160–220 Å; sample (5 + 5)rx, prepared without intermediate reduction, presents a lower crystallite size, in relation to a higher crystallite number, and thus better platinum precursor-support interactions. The higher average platinum size for samples 5r + 5rx and 3i.Pt.MF (i.e., with intermediate reduction at 400 °C) can be explained by the possibility of reaction of the first Pt crystallites (i.e., obtained after the first reduction) with the H_2PtCl_6 precursor.

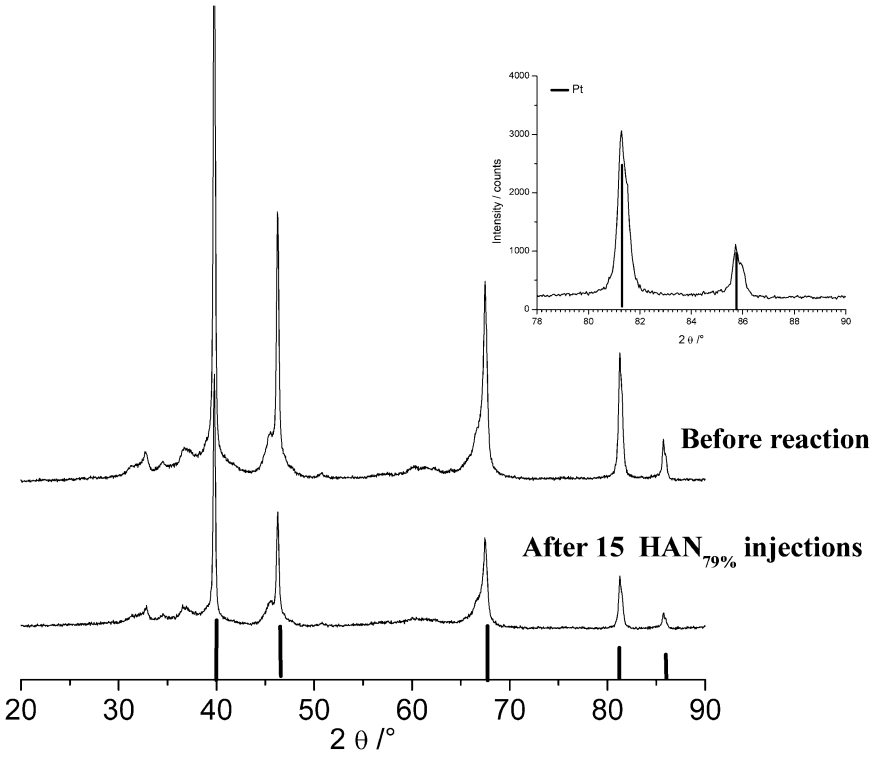

Fig. 6. Diffractograms of the 10rx catalyst before and after 15 injections of $HAN_{79\%}$ at 40 °C (enlargement to determine Pt particles size; ICDD file: 04-0802).

For two representative catalysts (5r + 5rx and (5 + 5)rx) the transmission electron microscopy images and the particle size distributions are indicated in Figs. 7a and 7b. The catalyst with intermediate reduction, 5r + 5rx, displays a very large distribution, whereas the second sample shows more numerous, smaller crystallites, in agreement with the XRD data. These extended particle size distributions are related to the high platinum percentage and low metal–support interactions. The volume-averaged size taken from these distributions was, respectively, 760 Å for 5r + 5rx and 170 Å for (5 + 5)rx samples. These average data are much higher than the values obtained from XRD, leading to the suspicious single crystal character of the largest particles. This point was corroborated by conical dark-field TEM images, with the use of (111) reflections (Fig. 7c), which obviously show that these particles are made of aggregates of smaller crystallites. Therefore the calculated volume-averaged value is overestimated. This concerns mainly the particles with a size greater than 200–300 Å.

3.4. Structural data and morphology: after reaction test

After the 15 HAN solution injections, the BET surface area remains of the same order of magnitude, except for the 5r + 5rx sample, which presents an area increase without structural change (same diffractograms for all samples; see Fig. 6). The XRD average size increases for one sample (10rx, Table 2).

After the reaction, the size distribution of sample 5r + 5rx (Fig. 7a) is explained by a dislocation of the platinum aggregates and an increase in the medium-sized crystallites; whereas sample (5 + 5)rx (Fig. 7b) displays a shift in the distribution of the nanosized particles. This is can be due to the loss of the smallest crystallites or to the formation of agglomerates; a sintering effect seems to be less probable at this low temperature, in agreement with the same XRD average size. The characteristics of the 10rx and 3i.Pt.MF catalysts are similar to those of the (5 + 5)rx sample. Nevertheless, for the 3i.Pt.MF sample, it was difficult to compare the sample before and after the reaction because of the breaking of the spheres.

All of the powdered samples displayed an important loss of platinum, about 40% detected after reaction (Table 2). This loss can be correlated with the presence of very small crystallites (Fig. 8a) on the carbon membrane of the copper grid used for the TEM experiment. To clarify this loss, we performed X-ray mapping on some catalysts (Figs. 9a and 9b). The 10rx catalyst shows the heterogeneity of a xerogel support with the presence of silica particles, as established in a previous work [11]. However, before the catalytic reaction, the platinum atom distribution appears to be almost homogeneous, and the content of platinum next to silica particles remains low (Fig. 9a). After the decomposition reaction, the presence of disconnected silica and platinum particles (Fig. 9b) is indicated. The heterogeneous distribution of platinum particles displays either the sintering of platinum crystallites or more probably the formation of nanosized platinum agglomerates (Fig. 8b). This effect confirms the possibility of platinum crystallite migration for the particles linked to silica groups. Moreover, these silica species

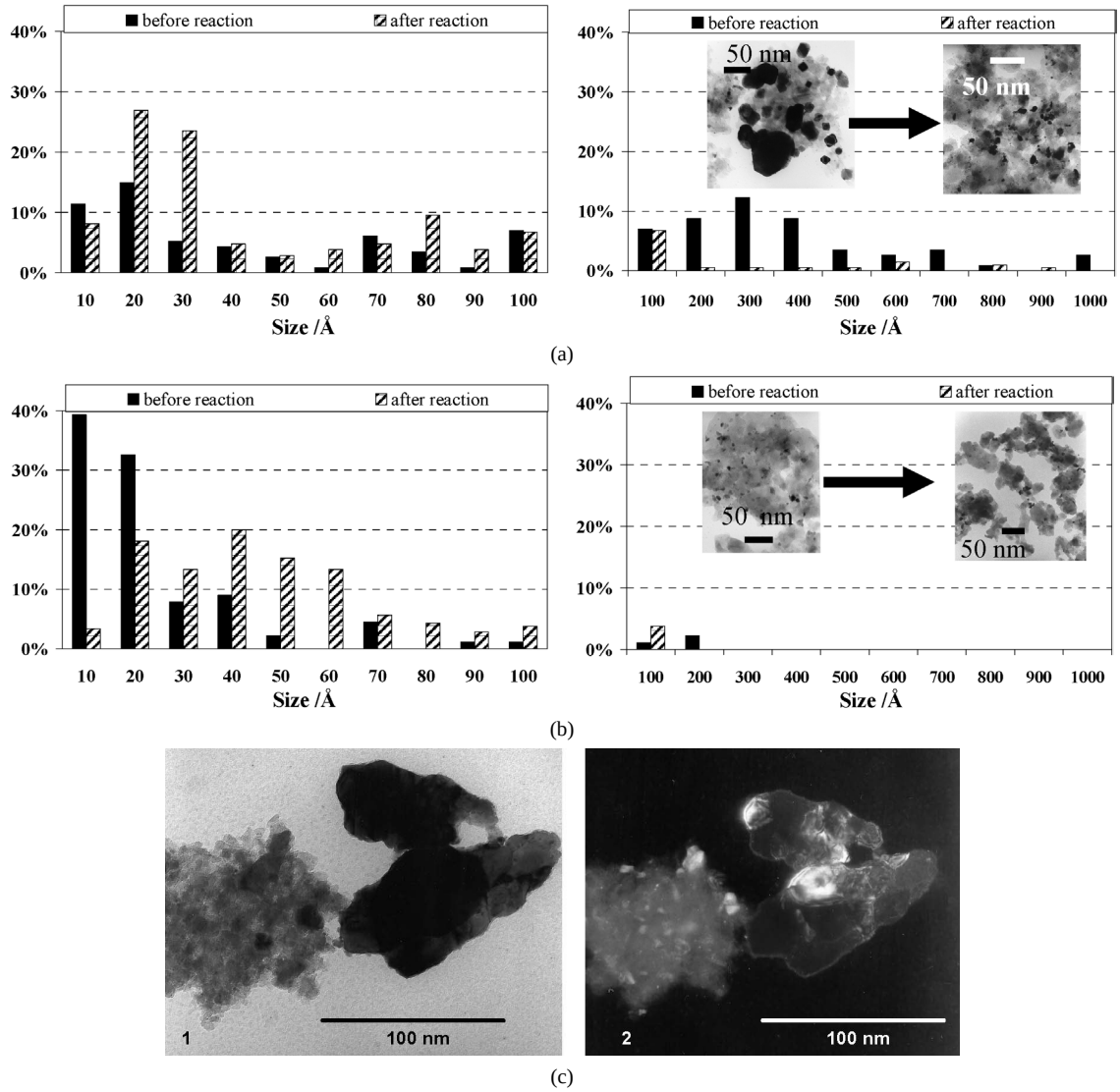

Fig. 7. Distributions of particles sizes deduced by transmission electron microscopy measurements (about 120 particles counted) and corresponding images before and after 15 injections of $HAN_{79\%}$ at 40 °C for the (a) and (5 + 5)rx (b) catalysts, (c) conical dark-field TEM images using 111 reflections of 5r + 5rx catalyst (1 bright field and 2 dark field).

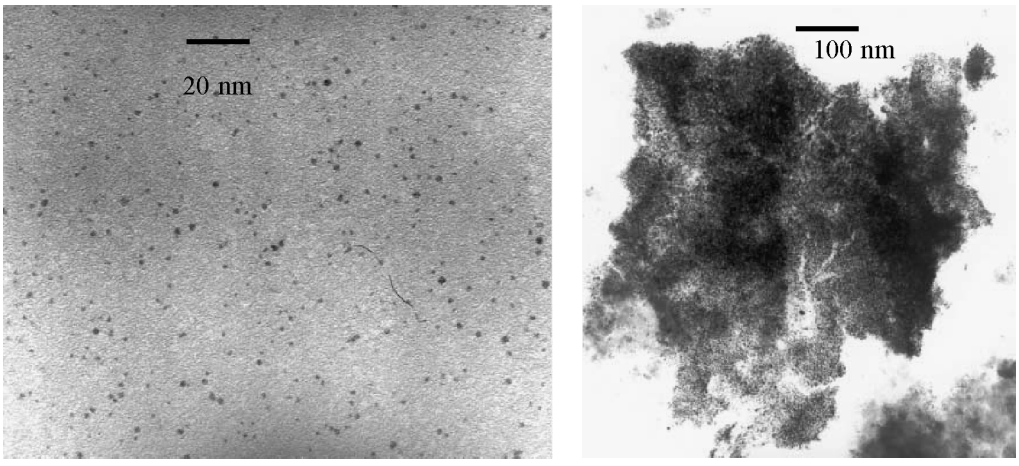

Fig. 8. Transmission electron microscopy images of the 10rx catalyst after 15 injections of $HAN_{79\%}$ at 40 °C: (a) platinum crystallites on membrane, (b) platinum agglomerates on catalyst.

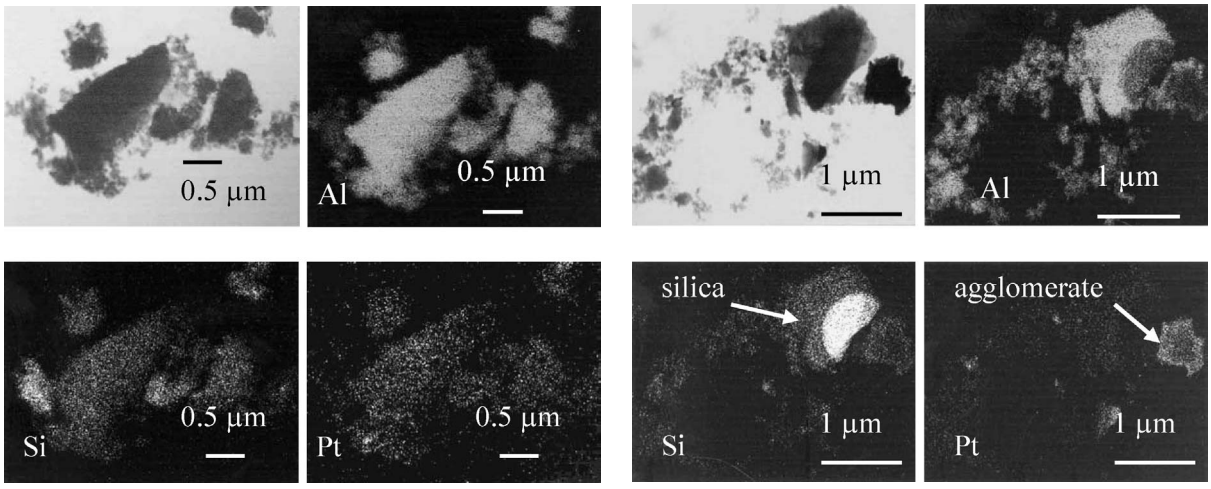

Fig. 9. X-ray mapping of 10rx catalyst (a) before and (b) after 15 injections of $HAN_{79\%}$ at 40 °C (Pt-L_α at 9.441 keV; Al-K_α at 1.486 keV; Si-K_α at 1.739 keV).

can be responsible for the primary loss of platinum in relation to the calculated values (i.e., sample 10rx: 8.3 instead of 10), which occurs during the catalyst preparation. Indeed, in this case the metal–support interactions are weaker for silica than for alumina [26,27]. This explanation provides an idea of the mechanism that occurs at the surface but does not explain the significant loss of platinum atoms. The platinum loss estimated from XRD data for sample 10rx (Fig. 6; intensity ratio of Pt diffraction peaks related to the diffraction peaks of alumina) is in the range of 10–20%; this value takes into account the largest crystallites, which remain preferentially on the support surface. This is in agreement with the observed slight increase in the XRD crystallite size (Table 2).

For more detailed explanations, experiments in water and in diluted nitric acid are being carried out to reproduce the conditions that occur in the batch reactor. These experiments consist of stirring a catalyst for 4 h in the presence of a neutral or nitric acid solution (pH ∼ 2.5) followed by filtration, to determine the platinum amount retrieved in solution. Only a very small amount of platinum (0.1%) is dissolved in the acidic solution, whereas no platinum could be detected in water. By comparison, after the catalytic decomposition, atomic absorption and ICP measurements revealed the presence of 6% initial platinum in solution. No aluminum or silicon could be detected, meaning that the support is not affected by the strong oxidizing feature of the reactant. Thus, the main loss of the platinum active phase is due to a dispersion of the nanosized platinum particles into the remaining solution or on the walls of the sample holder.

3.5. Proposed model

To clarify these results, we suggest a scheme considering the different possibilities for platinum species mobility under strong oxidizing conditions (Fig. 10). The surface of supported platinum on silicon-doped alumina catalysts consist of a theta alumina structure and silica and platinum

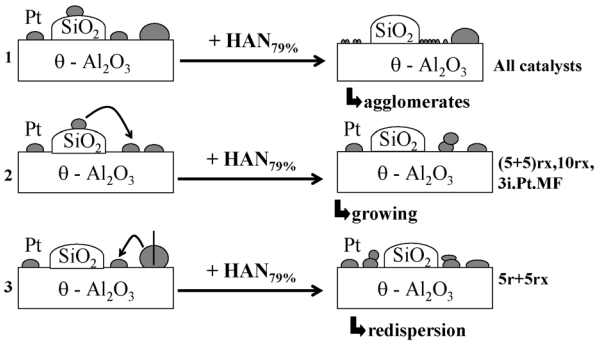

Fig. 10. Scheme displaying the transformation of platinum particles during the reaction of $HAN_{79\%}$ decomposition on catalysts.

particles. The platinum active phase is divided into three groups: (i) small particles fixed on alumina; (ii) small particles bonded to silica; and (iii) large aggregates on alumina. During the catalytic decomposition of the ionic liquid, the metallic species can react according to three possibilities (Fig. 10): (1) migration of platinum from silica to alumina, leading to the formation of nanosized platinum agglomerates deposited on the alumina surface; (2) migration of platinum from silica to another platinum particle, leading to growth; and (3) redispersion of the large platinum aggregates. These mechanisms are the results of strong reaction exothermicity, acidic and drastic oxidizing conditions, and energetic decomposition.

These mechanisms enable us to understand the catalytic results. Furthermore, the presence of platinum agglomerates may be related to the good activity of the catalysts. This argument can be correlated with the slope results. Indeed, we have shown that, up to the sixth or seventh injections, the catalyst is able to achieve an excellent performance. During this step, the formation of nanosized platinum agglomerates may occur. The metal species weakly linked to silica migrate into the aqueous solution, and the agglomerates are responsible for the reaction rate being maintained. In the case of metal-

lic aggregate dislocation (catalyst 5r + 5rx), the amount of small particles increases with the reaction rate and confirms that the agglomerates of very small crystallites are responsible for the good activity. It is important to remember that the best catalyst (5r + 5rx; Fig. 4) is a material that presents a value for the pressure slope higher than 500 mbar s^{-1}. But regarding the homogeneity, the reproducibility, the presence of nanometric platinum crystallites, and, more important, the decomposition behavior of HAN on these catalysts, as shown in Table 1 (25 °C, 129 mbar, 120 mbar s^{-1} for (5 + 5)rx), the best catalyst to consider is then the (5 + 5)rx sample.

4. Conclusions

This work shows that supported platinum on silicon-doped alumina catalyst is active and stable after 15 injections of a HAN-water mixture at 40 °C. The X-ray diffraction results confirm the presence of theta alumina structure without change after the catalytic reaction. Transmission electron microscopy images and size distribution confirm the heterogeneous distribution of silica and platinum particles. The activity is mainly due to the formation of nanosized platinum agglomerates responsible for the efficient decomposition of ionic liquid. During the catalytic decomposition, the low metal–silica interactions lead to a migration of the metallic particles, which are responsible for sintering of the smallest crystallites and dislocation of the aggregates. The suggested model relates to the surface change in the catalyst before and after the reaction. Two possibilities are discussed, one concerning the loss of platinum linked to silica particles and the other concerning a redistribution of platinum species.

Acknowledgments

We thank the European Space Agency (ESA-ESTEC, Noordwijk, the Netherlands), the French Space Agency (Centre National d'Etudes Spatiales, Toulouse, France) for funding this study as well as the 12th CPER (Contrat de plan Etat Region Poitou Charente, France) for funding the dynamic reactor.

References

[1] E.W. Schmidt, Hydrazine and Its Derivatives. Preparation, Properties, Applications, second ed., Wiley, New York, 2001, p. 2121.
[2] H.F.R. Schoyer, W.H.M. Welland-Veltmans, J. Louwers, P.A.O.G. Korting, A.E.D.M. van der Heijden, H.L.J. Keizers, R.P. van den Berg, J. Propulsion Power 18 (2002) 131.
[3] M. Farshchi, V. Vaezi, B.D. Shaw, Combustion Sci. Technol. 174 (2002) 71.
[4] Y.-P. Chang, K.K. Kuo, J. Propulsion Power 18 (2002) 1076.
[5] K. Anflo, T.A. Grönland, G. Bergman, M. Johansson, R. Nedar, Proc. 38th Joint Propulsion Conference, Indianapolis, IN, July 2002, AIAA Paper 2002-3847.
[6] B. Reed, S. Harasim, Proc. 37th Joint Propulsion Conference, Salt Lake City, UT, July 2001, AIAA Paper 2001-3696.
[7] R. Eloirdi, S. Rossignol, C. Kappenstein, D. Duprez, N. Pillet, J. Propulsion Power 19 (2003) 213.
[8] L. Courthéoux, R. Eloirdi, S. Rossignol, C. Kappenstein, D. Duprez, N. Pillet, Proc. 38th Joint Propulsion Conference, Indianapolis, IN, July 2002, AIAA Paper 2002-4027.
[9] H. Lee, T.A. Litzinger, Combution Flame 135 (2003) 151.
[10] E.W. Schmidt, D.F. Gavin, US Patent 5485722 (1996).
[11] L. Courthéoux, F. Popa, E. Gautron, S. Rossignol, C. Kappenstein, J. Non-Cryst. Solids 350 (2004) 113.
[12] S. Rossignol, C. Kappenstein, Int. J. Inorg. Mater. 3 (2001) 51.
[13] F. Popa, L. Courthéoux, E. Gautron, S. Rossignol, C. Kappenstein, Eur. J. Inorg. Chem. (2005) 543.
[14] AIAA papers are available from the American Institute for Aeronautics and Astronautics Website: http://www.aiaa.org/content.cfm?pageid=413.
[15] A.F. Popa, S. Rossignol, C. Kappenstein, J. Mater. Chem. 12 (2002) 2866.
[16] M. Nguefack, A.F. Popa, S. Rossignol, C. Kappenstein, Phys. Chem. Chem. Phys. 5 (2003) 4279.
[17] B.E. Yoldas, J. Mater. Sci. 10 (1975) 1856.
[18] B.E. Warren, X-Ray Diffraction, Dover, New York, 1969, p. 251.
[19] Y. Batonneau, L. Courthéoux, P. Esteves, L. Pirault-Roy, S. Rossignol, C. Kappenstein, N. Pillet, Proc. 40th Joint Propulsion Conference, Fort Lauderdale, FL, USA, July 2004, AIAA Paper 2004-3835.
[20] J. Schoppelrei, T. Brill, J. Phys. Chem. A 101 (1977) 8593.
[21] J. Cronin, T. Brill, J. Phys. Chem. A 90 (1986) 178.
[22] H. Lee, T. Litzinger, Combustion Flame 127 (2001) 2205.
[23] A. Roine, HSC Chemistry® for Windows, Chemical Reaction and Equilibrium Software with Extensive Thermochemical Database, Version 5.1, Outokumpu Research Oy, Pori, Finland, 2002, ISBN 952-9507-08-9.
[24] C. Wang, C. Yeh, Appl. Catal. A 209 (2001) 1.
[25] U. Olsbye, R. Wendelbo, D. Akporiaye, Appl. Catal. A 152 (1997) 127.
[26] A. Douidah, P. Marécot, S. Szabo, J. Barbier, Appl. Catal. A 225 (2002) 21.
[27] S. Jackson, G. Kelly, G. Webb, J. Catal. 176 (1998) 225.